Journal of Biomechanics 47 (2014) 3681–3688

Contents lists available at ScienceDirect

Journal of Biomechanics

journal homepage: www.elsevier.com/locate/jbiomech
www.JBiomech.com

A statistical geometrical description of the human liver for probabilistic occupant models

Yuan-Chiao Lu, Costin D. Untaroiu *

Department of Biomedical Engineering and Mechanics, Virginia Tech, Blacksburg, VA 24060, USA

ARTICLE INFO

Article history:
Accepted 25 September 2014

Keywords:
Human liver
Statistical shape model
Principal component analysis
Mean and boundary models

ABSTRACT

Realistic numerical assessments of liver injury risk for the entire occupant population require incorporating inter-subject variations into numerical models. Statistical shape models of the abdominal organs have been shown to be useful tools for the investigation of the organ variations and could be applied to the development of statistical computational models. The main objective of this study was to establish a standard procedure to quantify the shape variations of a human liver in a seated posture, and construct three-dimensional (3D) statistical shape boundary models.

Statistical shape analysis was applied to construct shape models of 15 adult human livers. Principal component analysis (PCA) was then utilized to obtain the modes of variation, the mean model, and a set of statistical boundary shape models, which were constructed using the *q*-hyper-ellipsoid approach.

The first five modes of a human liver accounted for the major anatomical variations. The modes were highly correlated to the height, thickness, width, and curvature of the liver, and the concavity of the right lobe. The mean model and the principal components were utilized to construct four boundary models of human liver. The statistical boundary model approach presented in this study could be used to develop probabilistic finite element (FE) models. In the future, the probabilistic liver models could be used in FE simulations to better understand the variability in biomechanical responses and abdominal injuries under impact loading.

1. Introduction

Statistical shape models (SSMs) have been shown to be valuable investigation tools into the variation in anatomical shapes (Barratt et al., 2008; Bischoff et al., 2014; Bredbenner et al., 2010; Chen and Shapiro, 2009; Davies et al., 2008; van de Giessen et al., 2010). SSMs of the abdominal organs could be used for the investigation of the organ variations for medical treatments (Okada et al., 2007; Reyes et al., 2010) and could also be applied to the development of computational probabilistic finite element (FE) models (Lu and Untaroiu, 2013; Untaroiu et al., 2012). Several previous studies have investigated the shape variations of the abdominal organs (e.g. liver, spleen, and kidney) (Chen and Shapiro, 2009; Davies et al., 2010; Lamecker et al., 2002; Reyes et al., 2010). However, none of these studies has examined the shape of these organs in an occupant posture and evaluated quantitatively the correspondence process used to choose the landmarks.

Statistical shape analysis (SSA) is a common technique to evaluate the size and shape variations. In recent SSA studies, the model registration, automatic landmark identification through correspondence process, and the principal component analysis (PCA) are included as major steps of the construction of 3D SSMs. The principal directions of variation, also called "modes of variation," could be represented by eigenvectors calculated from PCA (van de Giessen et al., 2010). Several studies have applied SSA on human soft tissues (Chen and Shapiro, 2009; Chen et al., 2010; Lamecker et al., 2002; Reyes et al., 2010), bones (Barratt et al., 2008; Bredbenner et al., 2010; Fripp et al., 2005; Lorenz and Krahnstover, 1999; van de Giessen et al., 2010), and the entire human body (Azouz et al., 2006; Xi et al., 2007). All of these studies utilized PCA to construct only the SSMs corresponding to main variation modes.

The shapes of solid abdominal organs may vary in different postures due to gravity (Beillas et al., 2009; Hayes et al., 2013). Beillas et al. (2009) showed that the solid abdominal organs (liver, kidney, and spleen) in the supine posture changed up to 40 mm when compared with the standing, seated, and forward-flexed postures. It was suggested that the abdominal geometries in different postures should be considered accordingly in FE simulations. Hayes et al. (2013) compared the location and morphology of abdominal organs between seated and supine postures. It was found that the liver in the seated posture expanded 7.8% cranially and compressed 3.4% and 5.2% in the anterior–posterior and

* Corresponding author. Tel.: +1 540 231 8997; fax: +1 540 231 2953.
E-mail address: costin@vt.edu (C.D. Untaroiu).

http://dx.doi.org/10.1016/j.jbiomech.2014.09.031
0021-9290/

medial–lateral directions, respectively. Similar results were found for the human spleen and kidney.

To automatically build SSMs from a training set of shapes, finding point correspondence across images becomes an essential task (Chen et al., 2010). Several correspondence approaches to determine the corresponding landmarks between shapes have been proposed and compared in literature (Chen and Shapiro, 2009; Dalal et al., 2007; He et al., 2009; Lamecker et al., 2002; Styner et al., 2003; van de Giessen et al., 2010). Dalal et al. (2007) proposed a correspondence approach, which established landmarks on a selected shape (template) and used the shortest distances between the template landmarks and the points on the target surfaces to determine the corresponding target landmarks. However, estimating corresponding points based merely on minimum Euclidean distance was found to be inaccurate in regions with large curvatures (Heimann and Meinzer, 2009). In addition, if the two aligned shapes do not have a certain amount of overlapping, the approach based on shortest distance may fail to establish the correct correspondence (He et al., 2009, 2010). To avoid these limitations, several improved correspondence algorithms were proposed using both coordinates and surface normal (Brett and Taylor, 2000; He et al., 2009; van de Giessen et al., 2009). The target landmark corresponding to each template landmark was defined as the surface point on a target surface with the smallest Euclidean distance and smallest difference between surface normals (He et al., 2009; van de Giessen et al., 2009). In addition, it was shown (Belongie et al., 2002) that the iterative thin-plate spline (TPS) algorithm (Bookstein, 1989) could efficiently refine the corresponding landmarks faster than the landmark sliding approach (Dalal et al., 2007) without loss of accuracy. Therefore, the correspondence approach considering the shortest distance and surface normals (He et al., 2009; van de Giessen et al., 2009) and the iterative TPS algorithm (Belongie et al., 2002) were applied in the current study.

The main objective of this study was to investigate the human liver geometrical variation in an occupant posture. The principal components which contributed more than 5% of the overall variation were presented. In addition, two efficient correspondence approaches were quantitatively compared according to three well-defined measures for shape-correspondence evaluation (Dalal et al., 2007; Lu et al., 2013). Finally, boundary models (Lu et al., 2013) of human liver in occupant posture were calculated to be later used in probabilistic FE simulations for developing a better understanding of the influence of liver geometric variation on the risk of occupant abdominal injuries and possibly, develop more advanced restraint systems.

2. Method

2.1. Segmentation

The shapes of human livers used to build the SSMs were reconstructed from the magnetic resonance imaging (MRI) scans of 15 subjects in a seated posture ("training set") (Beillas et al., 2009; Hayes et al., 2013) (Table 1). A point cloud of approximated 45,000 points on each liver surface was generated from the polygonal surfaces obtained by organ segmentation.

2.2. Registration

The position and orientation differences between organs were minimized such that the only remaining differences between the organs could be quantified by size and shape variations. One liver was selected as the "template", and the remaining 14 "target" liver models were registered to it. The liver model that is the closest to the mean geometry of all models under consideration is chosen as the template model (Joshi et al., 2004; Park et al., 2005). In the current study, the liver model of a 50th percentile male included in Hayes et al.' dataset was selected as the template. A popular robust registration approach, the Levenberg-Marquardt Iterated Closest Point (LM-ICP) technique, was implemented in this study. It has been shown (Fitzgibbon, 2003) that this approach allows the extension of ICP to use truly robust statistics with a concomitant reduction of dependence on the initial estimate.

Table 1
Demographic data of subjects.

Subject ID	Sex	Height (m)	Weight (kg)	Age (yr)	Source
F01	Female	1.74	68	41	Lyon
F02	Female	1.72	64	42	Lyon
F03	Female	1.62	53	34	Lyon
F04	Female	1.50	48	24	Wake
F05	Female	1.62	60.8	31	Wake
F06	Female	1.67	91.7	33	Wake
M01	Male	1.75	70	29	Lyon
M02	Male	1.91	88	32	Lyon
M03	Male	1.75	64	29	Lyon
M04	Male	1.69	60	26	Lyon
M05	Male	1.81	80	26	Lyon
M06	Male	1.83	82	37	Lyon
M07	Male	1.60	56.2	27	Wake
M08	Male	1.75	78.6	26	Wake
M09	Male	1.90	102.1	26	Wake

Note: "Lyon" refers to the dataset published by Beillas et al. (Beillas et al., 2009), and "Wake" refers to the dataset published by Hayes et al. (Hayes et al., 2013).

2.3. Correspondence

The correspondence process was performed to identify the landmarks on liver surfaces, which could be used for subsequent PCA. Three phases were involved in the establishment of landmarks on template and target surfaces: (1) establishment of the landmarks on the template surfaces; (2) establishment of surface normals for the landmarks on template surface and the points on target surfaces; and (3) establishment of the landmarks on the target surfaces.

The landmarks on the template surface were first constructed by the equal-size cubic grid method which divided the 3D space for the template surface into equal-size cubic grid cells (Dalal et al., 2007). For each cell containing surface points, the one closest to the center of this cell was picked as a landmark. A grid cell of $7\times7\times7$ mm^3 resulted in about 2100 template landmarks for each liver. The second phase was to find the surface normals of landmarks on the template surfaces and the randomly chosen points on the target surfaces. After establishing the surface normals, two correspondence approaches, the "He" approach (He et al., 2009) and the "Giessen" approach (van de Giessen et al., 2009), were utilized and compared for identifying the landmarks on the target surfaces.

In the "He" approach, the closest point from the target surface to a template landmark was assigned as the target landmark. If multiple closest points were identified, then the point with the closest surface normal to the template landmark was assigned as the target landmark. In the "Giessen" approach, the target landmark was identified as the surface point on a target model with the smallest Euclidean distance and weighted surface normal components to a certain template landmark in a six-dimensional space (van de Giessen et al., 2009).

After the initial corresponding landmarks between template and target surfaces were established, the quality of the target landmarks could be further improved by iterative TPS algorithm through transformation functions (Belongie et al., 2002; Bookstein, 1989; He et al., 2009). Five iterations were executed for each correspondence calculation between two surfaces. CPU time of about 90 min was required to obtain good corresponding landmarks between one template and 14 target liver surfaces using 5-iteration TPS algorithm (Microsoft Windows workstations equipped with Intel Core i5-2400 CPU at 3.10 GHz processors).

The goodness of correspondence was quantified using compactness, generalization, and specificity measures, widely applied in the literature (Dalal et al., 2007; Davies, 2002; Davies et al., 2010; Lu and Untaroiu, 2013; Munsell et al., 2008; Styner et al., 2003; van de Giessen et al., 2010). Detailed descriptions of these three measures could be found in Davies's study (Davies, 2002). A compact model is one that has slight variance and requires few parameters to define a shape instance. It is calculated as the cumulative variance of the modes of variation from PCA. The generalization ability of each model was measured from the training set using leave-one-out reconstruction. The experiment was carried out for $M=1,2,\ldots14$ modes of variation and repeated 15 times with different test shape selections for each mode M. A specific model should only generate instances that are similar to those in the training set. This property was accessed by generating 1000 instances based on the model which were then compared to the members of the training set by surface to surface distances. These measures for shape-correspondence evaluation were applied: (1) to investigate the effect of the chosen number of points on the target surfaces during the correspondence process (5000 vs. 10,000 vs. 20,000) and (2) to compare "He" and "Giessen" approaches for the shape-correspondence.

2.4. Principal component analysis and shape description

The modes of variation and the principal directions were computed using PCA, based on the established landmarks (Bredbenner et al., 2010; Chen et al., 2010;

Styner et al., 2003). The modes of variation are orthogonal and statistically independent. The percentage of variability of each mode can be defined as $\lambda_i/\Sigma_{i=1}^{N-1}\lambda_i$, where λ_i are the eigenvalues calculated from PCA and N is the number of livers. Typically, only the first few modes with large eigenvalues (i.e. large variance) describe major size and shape variations.

The mean model was determined as the average of the coordinates of the corresponding landmarks (Reed et al., 2009). Every model could be reconstructed by a linear combination of a subset of eigenvectors:

$$\hat{x} = \bar{x} + \sum_{i=1}^{q} \zeta_i e_i \quad (1)$$

where $\bar{x}$ is the mean shape, ζ_i are shape parameters, and e_i are the eigenvectors that describe the principal modes of size and shape variation. To satisfy the conditions for developing the SSMs, it is necessary to examine the normality of the principal component scores (van de Giessen et al., 2010). The scores for the modes were plotted as histograms, and their normality was tested using the Kolmogorov–Smirnoff tests (α=0.05).

For each mode of variation, fifty virtual shape models was developed from the mean model (i.e. mean shape) based on the normal distribution for each principal component (e.g. $\zeta_i = \rho\sqrt{\lambda_i}$, where ρ is a random number from a standard normal distribution). To visualize the shape variation induced by a corresponding mode of variation, the rest of shape parameters were kept constant (Azouz et al., 2006). Each mode of variation was linked visually to an intuitive shape variation (e.g. liver height) which was measured in all virtual models. The coefficient of correlation was calculated for each mode between the variations of shape parameter (ζ_i) and the corresponding shape variation chosen to represent the mode of variation.

2.5. Statistical boundary shape models

The mean model and the principal components calculated from PCA were utilized to construct the boundary models (Eq. (1)). The q-hyper-ellipsoid approach (Lu et al., 2013) was used to define the set of "κ% boundary models" corresponding to q principal modes (Fig. 1). If the distributions of the principal component scores are not significantly different from the normal distribution, the combination of the shape space [−1.96 SD, 1.96 SD] from pre-selected principal modes will cover 95% (κ%) of the total variance contributed by these q principal modes (SD: standard deviation) (Lu et al., 2013). For example, when the first three modes of variations are considered (q=3), the 3-hyper-ellipsoid equation of 95% boundary models (Fig. 1) is

$$\sum_{i=1}^{3} \frac{\zeta_i^2}{(1.96\sqrt{\lambda_i})^2} = 1 \quad (2)$$

In this study, the first five modes were considered (q=5), so the set of 95% boundary models was represented by a 5-hyper-ellipsoid equation

$$\sum_{i=1}^{5} \frac{\zeta_i^2}{(1.96\sqrt{\lambda_i})^2} = 1 \quad (3)$$

where ζ_i are

$$\begin{aligned}
\zeta_1 &= 1.96\sqrt{\lambda_1}\cos(\delta_1)\\
\zeta_2 &= 1.96\sqrt{\lambda_2}\sin(\delta_1)\cos(\delta_2)\\
\zeta_3 &= 1.96\sqrt{\lambda_3}\sin(\delta_1)\sin(\delta_2)\cos(\delta_3)\\
\zeta_4 &= 1.96\sqrt{\lambda_4}\sin(\delta_1)\sin(\delta_2)\sin(\delta_3)\cos(\delta_4)\\
\zeta_5 &= 1.96\sqrt{\lambda_5}\sin(\delta_1)\sin(\delta_2)\sin(\delta_3)\sin(\delta_4)
\end{aligned} \quad (4)$$

$0 \le \delta_i \le \pi$ when i=1,2,3, and $0 \le \delta_i < 2\pi$ when i=4.

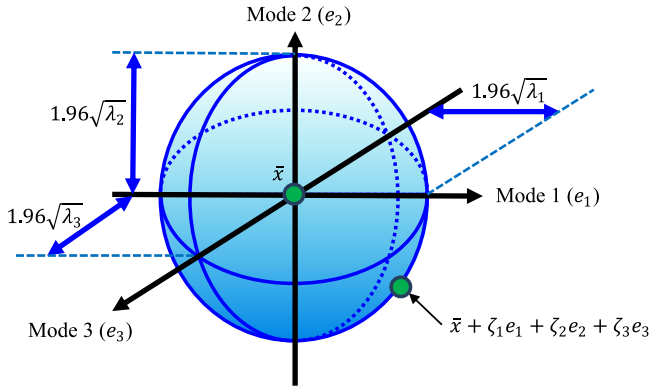

Fig. 1. An illustration of the set of 95% statistical boundary models developed using three pre-selected modes (q=3) (Lu et al., 2013).

3. Results

The compactness values of models constructed using "Giessen" approach based on 10,000 and 20,000 surface points were similar and smaller than the corresponding models with 5000 surface points (Fig. 2a). A similar trend was found for the generalization and specificity properties (Fig. 2b and c), indicating that 10,000 was a sufficient number of target surface points for constructing the liver SSMs.

Both "He" and "Giessen" approaches, using 10,000 target surface points (Fig. 3) required similar CPU time (90 min on Microsoft Windows workstations equipped with Intel Core i5-2400 CPU at 3.10 GHz processors) for determining the corresponding landmarks of all liver models. The values of the compactness, generalization, and specificity from "Giessen" approach were smaller than the corresponding values from "He" approach, indicating that the "Giessen" approach gave the better correspondence results (Fig. 3). Therefore, the "Giessen" correspondence approach and 10,000 target surface points were chosen to construct the mean and boundary models of the human liver in the current study.

Overall, the first five modes of the human liver shape analysis, which accounted for 73% of the total variation (Fig. 4), were chosen to graphically represent their corresponding SSMs (−3 SD, mean, and +3 SD) (Fig. 5). Measures corresponding to the shape changes in each principal direction were chosen (Fig. 5). Each measure correlated well with its corresponding mode of variation ($|r| > 0.99$, Fig. 6). The height of the liver corresponds to the first principal component which represented 30.7% of the global variance (Fig. 5, Mode 1). Variations in the liver thickness and width correlated to the second mode (Fig. 5, Mode 2), which represented 18.2% of the global variance. The third

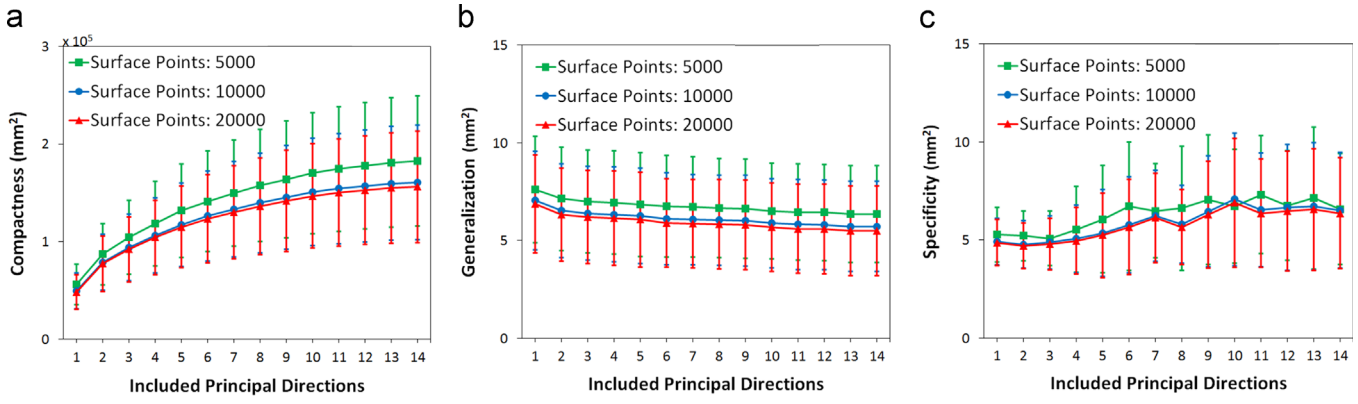

Fig. 2. Quantitative evaluation (compactness, generalization, and specificity) of shape-correspondence on human liver data between three numbers of surface points (Error bar: 1 SD). A smaller value for a certain number of included principal directions means a better approach.

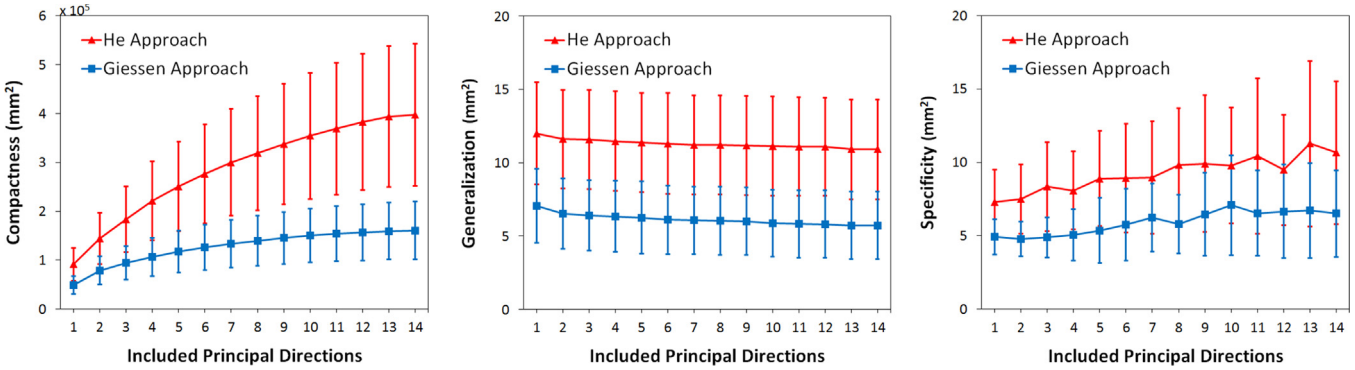

Fig. 3. Quantitative evaluation (compactness, generalization, and specificity) of shape-correspondence on human liver data between "He" method and "Giessen" method (Error bar: 1 SD). A smaller value for a certain number of included principal directions means a better approach.

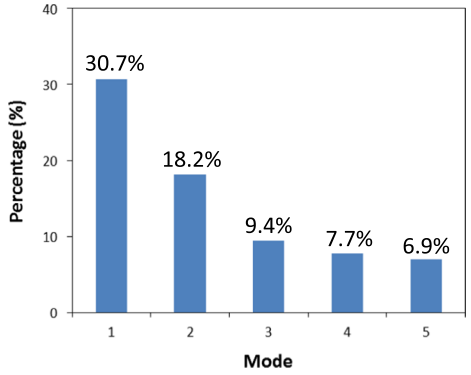

Fig. 4. Percentage of variation contributed by each mode for the human liver statistical size and shape model.

mode of variation represented 9.4% of the global variability and was highly correlated to the variation of the concavity of the right lobe (Fig. 5, Mode 3). The curvature of the liver, which represented 7.7% of the entire variance, was the main measure of the fourth mode of variation (Fig. 5, Mode 4). Finally, the height of left lobe corresponds to the variations in the fifth principal component, which accounts for 6.9% of the overall variation (Fig. 5, Mode 5).

All p-values from the Kolmogorov–Smirnoff tests on the similarity between the principal component scores and a standard normal distribution were greater than 0.05 (Fig. 7). This indicates that the distributions of the principal component scores were not significantly different from normal for all first five modes in human livers, so the principal components could be used in the development of SSMs.

The surfaces of four selected 95% boundary models of human livers were constructed (Fig. 8). These boundary models correspond to

$$(1)\ \delta_1=\delta_2=0,\quad \delta_3=\delta_4=\pi,\ \ (2)\ \delta_1=\delta_2=\delta_3=\delta_4=\pi/4,$$
$$(3)\ \delta_1=\pi/2,\delta_2=0,\ \ \delta_3=\pi/2,\ \ \delta_4=0,\ \ \text{and}$$
$$(4)\ \delta_1=\pi,\ \ \delta_2=\delta_3=\delta_4=0 \qquad (5)$$

4. Discussion

The current study fully investigated the liver shape variations based on seated posture models. The first two variation modes of liver shape presented in this study are different from the corresponding modes reconstructed from subjects in supine postures (Kohara et al., 2010; Lamecker et al., 2002). Kohara et al. used a relatively reduced number of the surface points (1000 vertex points) to express the liver training shapes. It was found that the size of the right lobe of the liver accounted for the first mode variation, and the size of the left lobe of the liver accounted for the second mode variation (Kohara et al., 2010). Using 12,500 surface points for each training shape, similar results were reported by Lamecker et al. (2002). The differences of the shape variations between these previous studies and current study could be explained by the shape changes of the abdominal organs due to gravitation between supine and seated postures reported previously (Beillas et al., 2009; Hayes et al., 2013) and/or by a different population. Other previous studies on liver shape models focused on the development of new correspondence methodologies (Chen and Shapiro, 2009) or multi-level SSA (Okada et al., 2007; Reyes et al., 2010), so the modes of variation were not clearly defined.

The volumes of mean and boundary liver models developed in this study (Fig. 5) were compared to the other similar data reported in literature (Fig. 9). The population-based studies (Heinemann et al., 1999; Vauthey et al., 2002) measured the liver volumes from Caucasian adults including both male and female subjects scanned at the supine posture. A previous study reported that the liver volume is unchanged in both supine and seated postures (Hayes et al., 2013). The volume of the mean model and the average volume of the ten ± 3 SD boundary models (Fig. 5) were both within ± 1 SD of the average liver volumes reported in population-based studies (Fig. 9). However, the volume of the male subject's liver recruited in Hayes' study, close to a 50th percentile male (Hayes et al., 2013), was significantly lower (Fig.9). This finding suggests that the development of a mean human model using SSA from a large population is a better approach than using a certain subject with an average overall anthropometry (Gayzik et al., 2011).

The current study shows that the "Giessen" approach performs better than the "He" approach in terms of the three measures of shape-correspondence evaluation. While the surface normal was considered in "He" approach, it was used only when multiple target surface points were initially chosen for a template landmark (He et al., 2009). This could induce some discrepancy of the surface normals between certain target landmarks and their corresponding template landmarks. Therefore, it is suggested to use the six-dimensional space of the combined coordinate and surface normal information of surface points to establish the corresponding landmarks between shapes (van de Giessen et al., 2010, 2009).

An optimization technique for improving the correspondence, called "iterative landmark sliding" (SLIDE), has shown to be better than other approaches such as minimum description length (MDL) and spherical harmonics (SPHARM), in terms of the three shape model evaluation measures (compactness, generalization, and specificity) (Dalal et al., 2009, 2007). While the SLIDE optimization was not considered in the current study, it has been shown that the correspondence map established using coordinates and surface normals along with iterative TPS to refine landmarks is sufficient

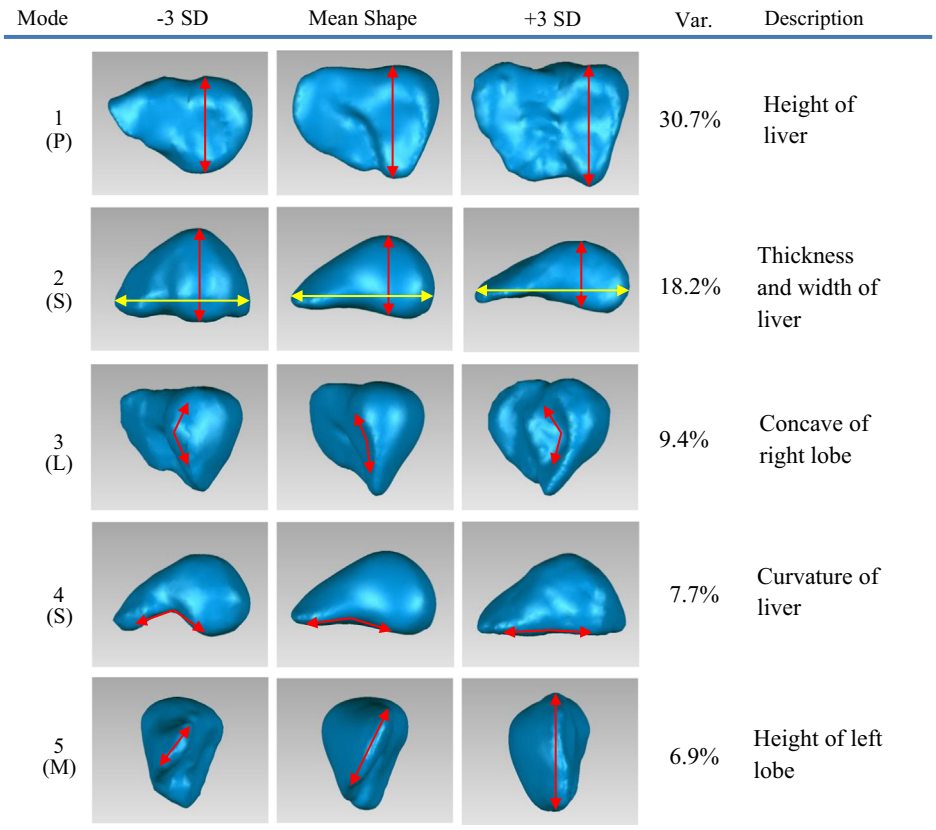

Fig. 5. The first five modes of variation of human livers. P: Posterior view; S: Superior view; L: Lateral view; and M: Medial view.

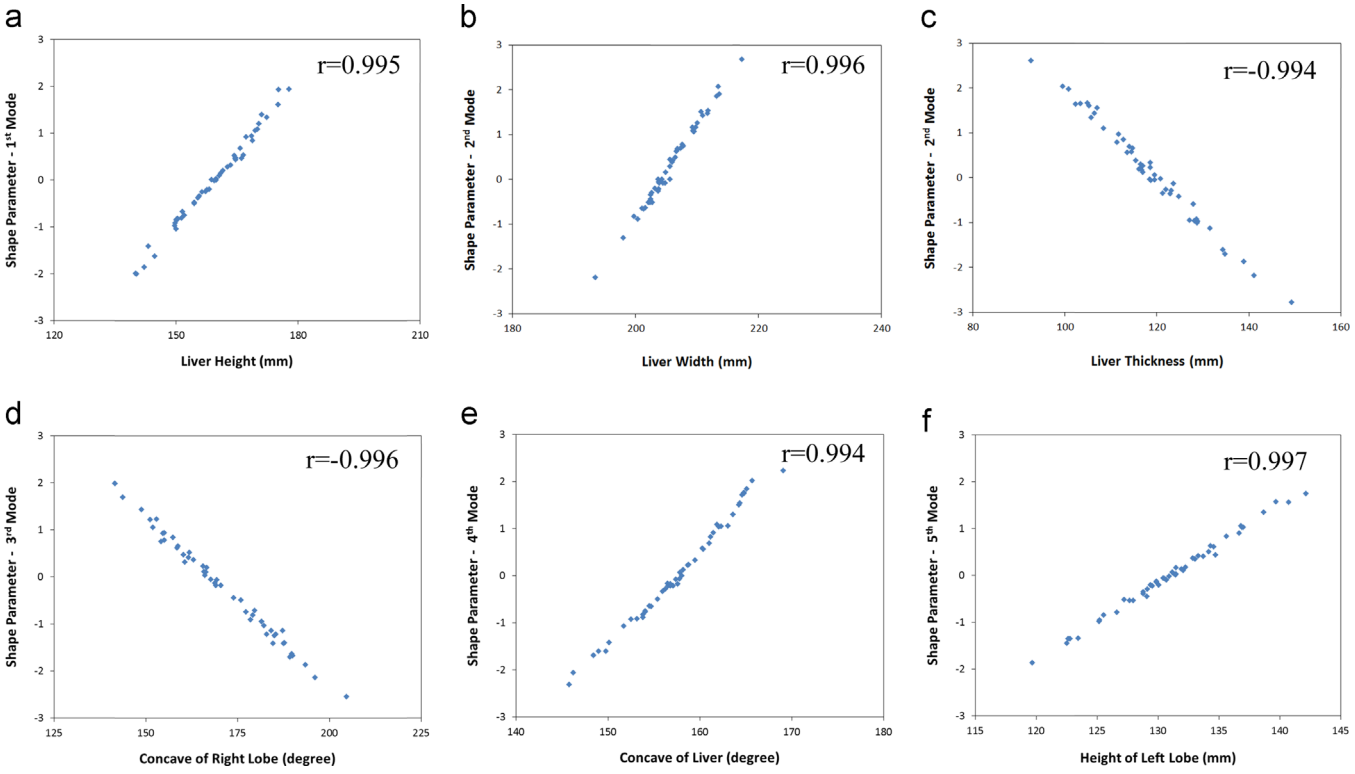

Fig. 6. Correlation between the variations of shape parameter (ζ_i) and shape changes for (a) Liver height (1st mode); (b) liver width (2nd mode); (c) liver thickness (2nd mode); (d) concave of right lobe (3rd mode); (e) concave of liver (4th mode); and (f) height of left lobe (5th mode). *Note*: r is the Pearson's correlation coefficient.

to obtain similar results of refined landmarks (He et al., 2010). In addition, the iterative TPS approach requires less computational time, and all the corresponding landmarks are on the original surface without sliding away (He et al., 2009, 2010). Therefore, considering efficiency and accuracy, the SLIDE optimization may not be required, but the comparison of correspondence maps with

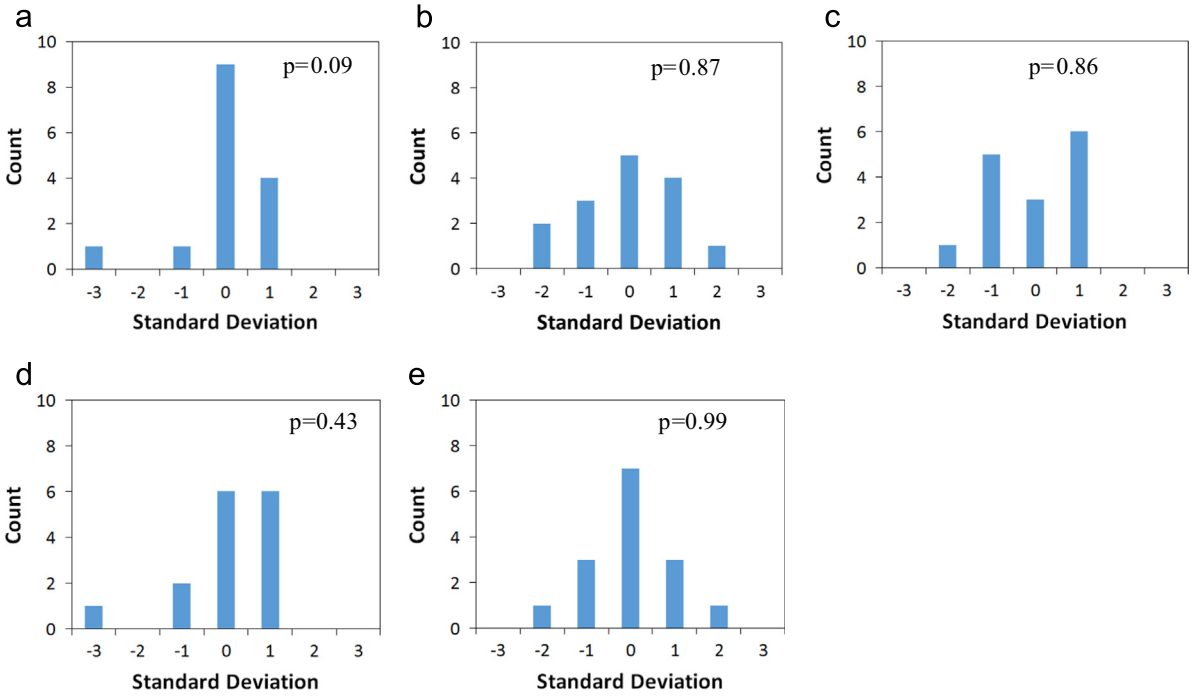

Fig. 7. Distributions of the principal component scores of the first five modes of human liver. p-values (p) > 0.05 represent normally distributed principal component scores.

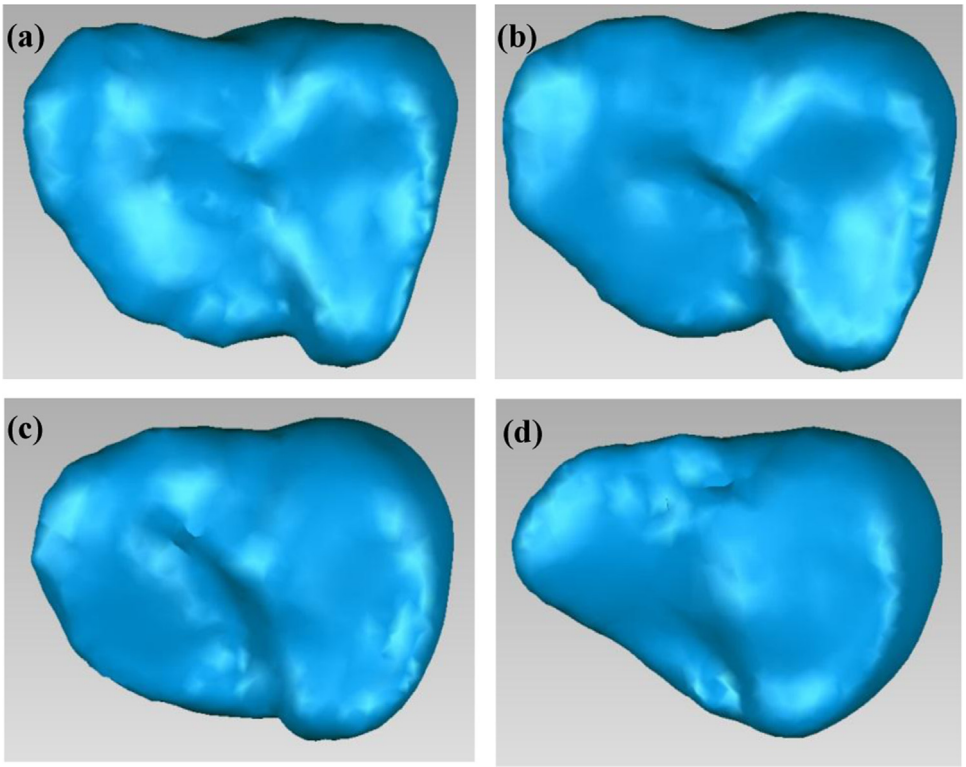

Fig. 8. Four selected boundary models of human liver, developed using the first five principal component modes (a) Boundary model #1; (b) Boundary model #2; (c) Boundary model #3; and (d) Boundary model #4.

SLIDE and without SLIDE is suggested to be investigated in future studies.

The shape variations between 95% liver boundary models (Fig. 8) indicate that the traditional scaling technique based on geometry parameters such as height and width may not be suitable for constructing percentile anthropometric models. This scaling technique has been extensively applied in crash test dummies (Untaroiu et al., 2008; Vezin and Verriest, 2005). The mesh of HUMOS2 model was scaled to any percentile in driving position through only 10 (external) parameters (Vezin and Verriest, 2005). The Polar-II FE model was scaled in the vertical direction to match the stature (height) and in the transverse plane to match the total mass between the pedestrian dummy model and subjects, in order to create 5th percentile female, 50th percentile female, and 95th percentile male FE models (Untaroiu et al., 2008). The proposed boundary models in the current study

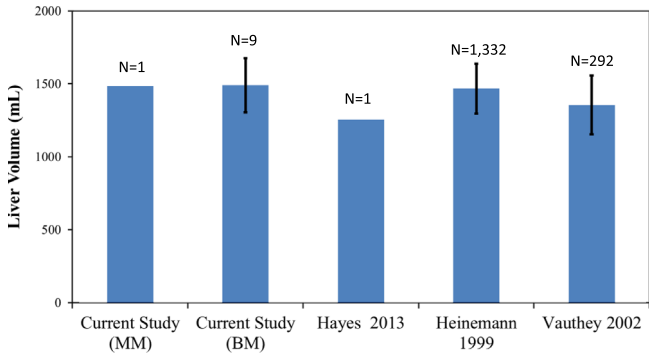

Fig. 9. Comparison of the liver volumes between current and previous studies. Error bar: 1 SD. MM – mean model and BM – boundary models.

provide a better perspective on human variations than the traditional percentile models.

One limitation in this study is that the liver was treated as a homogeneous material, which is typical in a majority of human FE models (Gayzik et al., 2011; Shin et al., 2012; Untaroiu et al., 2009, 2013; Yue and Untaroiu, 2014). However, robust universal relationships between medical images and material property of abdominal organs have not been published yet. Therefore, the incorporation of the density information from medical images into SSA may not be applicable at this time. Furthermore, the Kolmogorov–Smirnoff tests used for the examination of the normality of the shape parameters may be influenced by the relative small sample size. This is especially true when marginal significance is observed (e.g. p-value = 0.09). To better cover the whole human population, a larger sample size and gender/age effects should be taken into account in future studies by applying the same methodology presented in this study

The current study focuses on the size and shape variations of the liver itself. The location and orientation of the liver relative to other body tissues (e.g. spleen and kidney) could be obtained by extending the concept of the shape analysis to a larger scale. For example, some studies have applied the SSA to whole body scale to discover the variations of the relative positions and orientations between body segments (Azouz et al., 2006; Wuhrer et al., 2011; Xi et al., 2007). This could be a critical topic for future research to connect size and shape FE models of internal organs and bones. In addition, the size and shape models of the human liver could be further combined with distributions of liver material properties (Lu et al., 2014; Untaroiu et al., 2014) to develop probabilistic FE models of the liver (Laz and Browne, 2010). Using these probabilistic FE human models in impact simulations could help to better understand the variability observed in biomechanical and injury response of the abdominal organs under impact loading (Untaroiu, 2010; Untaroiu et al., 2012), to improve future anthropometric test devices (ATDs) used in compliant and regulatory testing (Parent et al., 2013; Putnam et al., 2014; Ridella and Parent, 2011), and probably to design advanced restraint systems which may take into account the occupant anthropometry (Adam and Untaroiu, 2011; Untaroiu and Adam, 2013).

Conflict of interest statement

There is no conflict of interest in this study.

Acknowledgments

The authors thank Dr. Philippe Beillas and Dr. Scott Gayzik for sharing the liver surfaces used in the current study.

References

Adam, T., Untaroiu, C.D., 2011. Identification of occupant posture using a Bayesian classification methodology to reduce the risk of injury in a collision. Transp. Res. Part C: Emerg. Technol. 19 (6), 1078–1094.
Azouz, Z.B., Rioux, M., Shu, C., Lepage, R., 2006. Characterizing human shape variation using 3D anthropometric data. Vis. Comput. 22 (5), 302–314.
Barratt, D.C., et al., 2008. Instantiation and registration of statistical shape models of the femur and pelvis using 3D ultrasound imaging. Med. Image Anal. 12 (3), 358–374.
Beillas, P., Lafon, Y., Smith, F.W., 2009. The effects of posture and subject-to-subject variations on the position, shape and volume of abdominal and thoracic organs. Stapp Car Crash J. 53, 127–154.
Belongie, S., Malik, J., Puzicha, J., 2002. Shape matching and object recognition using shape contexts. IEEE Trans. Pattern Anal. Mach. Intell. 24 (4), 509–522.
Bischoff, J.E., Dai, Y., Goodlett, C., Davis, B., Bandi, M., 2014. Incorporating population-level variability in orthopedic biomechanical analysis: a review. J. Biomech. Eng. 136 (2), 021004.
Bookstein, F.L., 1989. Principal warps: thin-plate splines and the decomposition of deformations. IEEE Trans. Pattern Anal. Mach. Intell. 11 (6), 567–585.
Bredbenner, T.L., et al., 2010. Statistical shape modeling describes variation in tibia and femur surface geometry between control and incidence groups from the osteoarthritis initiative database. J. Biomech. 43 (9), 1780–1786.
Brett, A.D., Taylor, C.J., 2000. A method of automated landmark generation for automated 3D PDM construction. Image Vis. Comput. 18 (9), 739–748.
Chen, J.-H., Shapiro, L.G., 2009. 3D point correspondence by minimum description length with 2DPCA. In: Proceedings of the IEEE Annual International Conference of the Engineering in Medicine and Biology Society, pp. 5657–5660.
Chen, J.-H., Zheng, K.C., Shapiro, L.G., 2010. 3D point correspondence by minimum description length in feature space. In: Proceedings of the 11th European Conference on Computer Vision: Part III. Springer-Verlag, Heraklion, Crete, Greece, pp. 621–634.
Dalal, P., et al., 2009. 3D open-surface shape correspondence for statistical shape modeling: Identifying topologically consistent landmarks. In: Proceedings of the IEEE 12th International Conference on Computer Vision, pp. 1857–1864.
Dalal, P., et al., 2007. A fast 3D correspondence method for statistical shape modeling. In: Proceedings of the IEEE Conference on Computer Vision and Pattern Recognition, CVPR '07, pp. 1–8.
Davies, R.H., 2002. Learning Shape: Optimal Models for Analysing Natural Variability. University of Manchester, Manchester, United Kingdom.
Davies, R.H., Twining, C.J., Cootes, T.F., Taylor, C.J., 2010. Building 3-D statistical shape models by direct optimization. IEEE Trans. Med. Imaging 29 (4), 961–981.
Davies, R.H., Twining, C.J., Taylor, C.J., 2008. Statistical Models of Shape: Optimisation and Evaluation. Springer Publishing Company, New York, NY (incorporated).
Fitzgibbon, A.W., 2003. Robust registration of 2D and 3D point sets. Image Vis. Comput. 21 (13–14), 1145–1153.
Fripp, J., et al., 2005. 3D statistical shape models to embed spatial relationship information. In: Proceedings of the 1st International Workshop on Computer Vision for Biomedical Image Applications, pp. 51–60.
Gayzik, F.S., et al., 2011. Development of a full body CAD dataset for computational modeling: a multi-modality approach. Ann. Biomed. Eng. 39 (10), 2568–2583.
Hayes, A.R., Gayzik, F.S., Moreno, D.P., Martin, R.S., Stitzel, J., 2013. Comparison of organ location, morphology, and rib coverage of a midsized male in the supine and seated positions. Comput. Math. Methods Med. 2013, 419821.
He, Q., et al., 2009. Detecting 3D corpus callosum abnormalities in phenylketonuria. Int. J. Comput. Biol. Drug Des. 2 (4), 289–301.
He, Q., Duan, Y., Karsch, K., Miles, J., 2010. Detecting corpus callosum abnormalities in autism based on anatomical landmarks. Psychiatry Res. 183 (2), 126–132.
Heimann, T., Meinzer, H.-P., 2009. Statistical shape models for 3D medical image segmentation: a review. Med. Image Anal. 13 (4), 543–563.
Heinemann, A., Wischhusen, F., Püschel, K., Rogiers, X., 1999. Standard liver volume in the Caucasian population. Liver Transplant. Surg. 5 (5), 366–368.
Joshi, S., Davis, B., Jomier, M., Gerig, G., 2004. Unbiased diffeomorphic atlas construction for computational anatomy. Neuroimage 23 (1), S151–S160.
Kohara, S., et al., 2010. Application of statistical shape model to diagnosis of liver disease. In: Proceedings of the 2nd International Conference on Software Engineering and Data Mining, SEDM , pp. 680–683.
Lamecker, H., Lange, T., Seebass, M., 2002. A statistical shape model for the liver. In: Proceedings of the 5th International Conference on Medical Image Computing and Computer-Assisted Intervention-Part II, pp. 421–427.
Laz, P.J., Browne, M., 2010. A review of probabilistic analysis in orthopaedic biomechanics. Proc. Inst. Mech. Eng. H 224 (8), 927–943.
Lorenz, C., Krahnstover, N., 1999. 3D statistical shape models for medical image segmentation. In: Proceedings of the Second International Conference on 3-D Digital Imaging and Modeling, pp. 414–423.
Lu, Y.-C., Kemper, A.R., Untaroiu, C.D., 2014. Effect of storage on tensile material properties of bovine liver. J. Mech. Behav. Biomed. Mater. 29 (0), 339–349.
Lu, Y.-C., Untaroiu, C.D., 2013. Statistical shape analysis of clavicular cortical bone. Comput. Methods Programs Biomed. 111 (3), 613–628.
Lu, Y.-C., Untaroiu, C.D., Kemper, A.R., Gayzik, S., Beillas, P., 2013. Statistical modeling of human liver incorporating the variations in shape, size, and material properties. Stapp Car Crash J. 57, 285–311.

Munsell, B.C., Dalal, P., Song, W., 2008. Evaluating shape correspondence for statistical shape analysis: a benchmark study. IEEE Trans. Pattern Anal. Mach. Intell. 30 (11), 2023–2039.

Okada, T., et al., 2007. Automated segmentation of the liver from 3D CT images using probabilistic atlas and multi-level statistical shape model. In: Ayache, N., Ourselin, S., Maeder, A. (Eds.), Medical Image Computing and Computer-Assisted Intervention – MICCAI 2007. Lecture Notes in Computer Science. Springer, Berlin, Heidelberg, pp. 86–93.

Parent, D.P., Craig, M., Ridella, S.A., McFadden, J.D., 2013. Thoracic biofidelity assessment of the THOR Mod Kit ATD. In: Proceedings of the 23rd International Technical Conference on the Enhanced Safety of Vehicles (ESV).

Park, H., Bland, P.H., Hero, A.O.R., Meyer, C.R., 2005. Least biased target selection in probabilistic atlas construction. Med. Image Comput. Comput. Assist. Interv. 8 (2), 419–426.

Putnam, J.B., Somers, J.T., Untaroiu, C.D., 2014. Development, calibration, and validation of a head-neck complex of THOR mod kit finite element model. Traffic Inj. Prev. 15 (8), 844–854.

Reed, M.P., Sochor, M.M., Rupp, J.D., Klinich, K.D., Manary, M.A., 2009. Anthropometric specification of child crash dummy pelves through statistical analysis of skeletal geometry. J. Biomech. 42 (8), 1143–1145.

Reyes, M., González Ballester, M.A., Kozic, N., Summers, R.M., Linguraru, M.G., 2010. Hierarchical patch generation for multilevel statistical shape analysis by principal factor analysis decomposition, Proc. SPIE 7626, Medical Imaging 2010: Biomedical Applications in Molecular, Structural, and Functional Imaging, 762617, San Diego, CA, pp. 762617-1–762617-8.

Ridella, S.A., Parent, D.P., 2011. Modifications to improve the durability, usability and biofidelity of the THOR-NT dummy. In: Proceedings of the 22nd ESV Conference. Washington, D.C., USA.

Shin, J., Yue, N., Untaroiu, C.D., 2012. A finite element model of the foot and ankle for automotive impact applications. Ann. Biomed. Eng. 40 (12), 2519–2531.

Styner, M.A., et al., 2003. Evaluation of 3D correspondence methods for model building. In: Proceedings of the Conference on Information Processing in Medical Imaging, 18, pp. 63–75.

Untaroiu, C.D., 2010. A numerical investigation of mid-femoral injury tolerance in axial compression and bending loading. Int. J. Crashworth. 15 (1), 83–92.

Untaroiu, C.D., Adam, T.J., 2013. Performance-based classification of occupant posture to reduce the risk of injury in a collision. IEEE Trans. Intell. Transp. Syst. 14 (2), 565–573.

Untaroiu, C.D., et al., 2012. Effect of seat belt pretensioners on human abdomen and thorax: biomechanical response and risk of injuries. J. Trauma Acute Care Surg. 72 (5), 1304–1315.

Untaroiu, C.D., et al., 2009. Experimental and computational investigation of human clavicle response in anterior–posterior bending loading – biomed 2009. Biomed. Sci. Instrum. 45, 6–11.

Untaroiu, C.D., Lu, Y.C., Siripurapu, S.K., Kemper, A.R., 2014. Modeling the biomechanical and injury response of human liver parenchyma under tensile loading. J. Mech. Behav. Biomed. Mater..

Untaroiu, C.D., et al., 2008. A study of the pedestrian impact kinematics using finite element dummy models: the corridors and dimensional analysis scaling of upper-body trajectories. Int. J. Crashworth. 13 (5), 469–478.

Untaroiu, C.D., Yue, N., Shin, J., 2013. A finite element model of the lower limb for simulating automotive impacts. Ann. Biomed. Eng. 41 (3), 513–526.

van de Giessen, M., et al., 2010. Statistical descriptions of scaphoid and lunate bone shapes. J. Biomech. 43 (8), 1463–1469.

van de Giessen, M., et al., 2009. A statistical description of the articulating ulna surface for prosthesis design. In: Proceedings of the IEEE International Symposium on Biomedical Imaging: From Nano to Macro, ISBI '09, pp. 678–681.

Vauthey, J.N., et al., 2002. Body surface area and body weight predict total liver volume in Western adults. Liver Transplant. 8 (3), 233–240.

Vezin, P., Verriest, J.P., 2005. Development of a set of numerical human models for safety. In: Proceedings of the 19th International Technical Conference on the Enhanced Safety of Vehicles.

Wuhrer, S., Shu, C., Xi, P., 2011. Landmark-free posture invariant human shape correspondence. Vis. Comput. 27 (9), 843–852.

Xi, P., Lee, W.-S., Shu, C., 2007. Analysis of segmented human body scans. In: Proceedings of Graphics Interface 2007. ACM, Montreal, Canada, pp. 19–26.

Yue, N., Untaroiu, C.D., 2014. A numerical investigation on the variation of hip injury tolerance with occupant posture during frontal collisions. Traffic Inj. Prev. 15 (5), 513–522.